ACTIVE CONTROL OF TAYLOR-GÖTLER VORTICES IN TURBULENT CURVED CHANNEL FLOW

Chun-Xiao Xu, Zhaoshun Zhang
Department of Engineering Mechanics,
Tsinghua University
Beijing 100084, China
xucx@tsinghua.edu.cn

Jung-Il Choi, Hyung Jin Sung
Department of Mechanical Engineering,
Korea Advanced Institute of Science and Technology,
373-1,Kusong-dong, Yusong-gu, Taejon, 305-701, Korea

ABSTRACT

Active control of Taylor-Götler vortices in turbulent curved channel flow is studied by direct numerical simulations. The drifting Taylor-Götler vortices are identified by a new proposed algorithm which is based on the wavelet transform of the wall information. The opposition control similar to Choi, Moin & Kim (1994) is applied to a turbulent curved channel flow to attenuate the large scale Taylor-Götler vortices and the attendant small scale vortices near the wall. Several active cancellations are tested to assess the effectiveness of the controls. It is found that a combined active cancellation at the concave wall makes the Taylor-Götler vortices break up to smaller vortices and weaken their strengths and contributions to Reynolds stress.

INTRODUCTION

Turbulent flow with streamline curvature is of considerable engineering interest. Taylor-Götler vortex is the characteristic flow structure closely related with concave streamline curvature. Although the geometry of a concave wall is not very complex, the boundary layer that develops on its surface is difficult to model due to the presence of streamwise Taylor-Götler vortices (Lund, 1996). The presence of Taylor-Götler vortices makes the flow on a concave wall to be three-dimensional rather than two-dimensional. Bradshaw's comprehensive review of effects of longitudinal streamline curvature on turbulent flow is that the effect of any extra rates of strain, such as that imposed by streamline curvature, is often an order of magnitude more important than the explicit effects of the extra tethat appear in the equations of motion (Bradshaw, 1973).

Taylor-Götler vortices were first studied as a kind of flow stability problem (Götler, 1940). The boundary layer instabilities induced by wall curvature were reviewed by Saric (Saric, 1994). A literature survey reveals that many experimental and numerical studies have been made on Taylor-Götler vortices in turbulent flows over concave surfaces (Patel & Sotiropolous, 1997). Taylor-Götler vortices are very important in the establishment of the asymmetry between the concave and convex walls in the curved channel. Moser & Moin (1987) found that Taylor-Götler vortices make a significant contributions to the concave-side Reynolds stress, but they contribute negligibly to the convex side. The induced upwash and downwash motions serve as effective agents to transport streamwise momentum normal to the wall, thereby increasing the skin friction. The secondary flow induced by wall curvature is then very closely related with the generation of skin friction drag (Lund & Moin, 1996).

Choi, Moin & Kim (1994) investigated an active control strategy for the purpose of drag reduction in turbulent channel flow. The control algorithm is based on the input velocity at the wall, which is proportional and opposite to the instantaneous velocity at a location near the wall. By controlling either the normal or the spanwise velocity at the wall, they achieved $20-30\%$ reduction in the skin friction. In present study, a similar control algorithm is applied to a turbulent curved channel flow to attenuate the large scale Taylor-Götler vortices and the attendant small scale vortices near the wall. Several active cancellations are tested to assess the effectiveness of the controls. It is found that a combined active cancellation at the concave wall makes the Taylor-Götler vortices break up to smaller vortices and weaken their strengths and contributions to Reynolds stress.

DIRECT NUMERICAL SIMULATION

A direct numerical simulations of turbulent curved channel flow is performed. Fig. 1 shows a schematic diagram of the flow domain and the coordinate system. The flow domain is a sector between two concentric cylinders. We use r, θ and z to denote the radial, azimuthal and axial directions respectively. As shown in Fig. 1, $R = (R_i + R_o)/2$ is the mean radius, $H = (R_o - R_i)/2$ is the half channel width, where R_i and R_o are the radius of the inner and outer cylinders, respectively. The ratio $\epsilon = H/R$ is defined as the curvature parameter.

The three-dimensional time-dependent incompressible Navier-Stokes equations are solved by a spectral method. To employ Chebyshev polynomials and Fourier series, the (r, θ, z) coordinates are transformed into (x, y, z) coordinates by

$$x = -\frac{R\theta}{H}, \quad y = \frac{r-R}{H}, \quad z = \frac{z}{H}, \tag{1}$$

with

$$x \in [0, L_x], \quad y \in [-1, 1], \quad z \in [0, L_z]. \tag{2}$$

Here $L_x = 2\pi/\alpha$, $L_z = 2\pi/\beta$. α and β are the basic wave numbers in x and z directions. The flow is driven by the

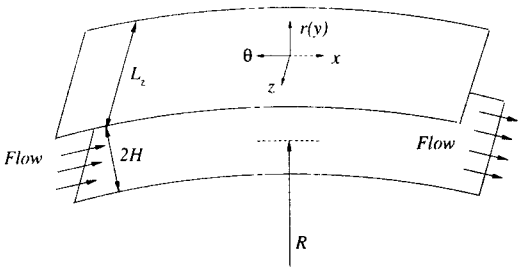

Figure 1: Flow geometry and coordinate system.

mean pressure gradient in x direction. x, y and z are referred to as streamwise, wall normal and spanwise directions, respectively. The corresponding velocity components are u, v and w.

A Chebyshev-collocation method is used in the wall normal direction and a dealiased Fourier-Galerkin method is adopted in the streamwise and spanwise directions for the spatial discretization. A third-order time-splitting method is employed to carry out the time advancement (Karniadakis, Israeli & Moin, 1991). Periodic conditions are used in streamwise and spanwise directions, and no-slip conditions are applied at the walls. All the simulations are performed with constant streamwise mass flux. The control to the flow through blowing and suction or sliding at the wall is realized by direct consideration of the wall boundary conditions (Choi, Moin & Kim, 1994). The Reynolds number is $Re_m = 2600$ based on the bulk mean velocity U_m and channel half width H. The curvature parameter is chosen as $\epsilon_1 = 0.0127$, which is the same as Moser & Moin (1987). The domain extends to $4\pi \times 2 \times 8\pi/3$ in the streamwise, wall-normal and spanwise directions, in concert with a grid size of $64 \times 64 \times 64$. For the validation of the domain size, the correlation functions are compared with those of Moser & Moin (1987). In wall units, the effective grid spacing is $\Delta x_c^+ = R^+\Delta\theta = 36$ in the streamwise direction and $\Delta z^+ = 12$ in the spanwise direction. In the radial direction, the maximum grid spacing is $\Delta y^+_{max} = 8.2$. A time step of $\Delta t = 0.01H/U_m$ is used in the present simulation.

Due to the existence of Taylor-Götler vortices, two types of averaging are employed in the present study. Supposing q is a flow quantity, we use $\bar{q} =< q >_{x,z,t}$ to denote the average in x, z and t, and $\tilde{q} =< q >_{x,t}$ to denote the average in just x and t. Hence $\tilde{q} - barq$ describes the state of Taylor-Götler vortices. The fluctuations of q with respect to $\bar{q}$ is defined as $q' = q - \bar{q}$ and referred to as total turbulence, while the fluctuations with respect to $\tilde{q}$ is defined as $q'' = q - \tilde{q}$ and referred to as underlying turbulence. It is obvious that $q' - q'' = \tilde{q} - \bar{q}$.

Because of the asymmetry of the curved channel with respect to the channel centreline, the wall values at the convex and concave walls are different (Moser & Moin, 1987). The shear stress at the convex wall (inner wall) is

$$\tau_i = \left(\frac{1}{Re}\frac{d\bar{u}}{dy}\right)_{y=-1}, \tag{3}$$

while the shear stress at the concave wall (outer wall) is

$$\tau_o = \left(\frac{1}{Re}\frac{d\bar{u}}{dy}\right)_{y=1}. \tag{4}$$

The mean streamwise pressure gradient to maintain a constant mass flux can be determined by

$$\frac{\partial\bar{p}}{\partial x} = \frac{(1-\epsilon)^2\tau_i + (1+\epsilon)^2\tau_o}{2} \tag{5}$$

Accordingly, three different wall friction velocity can be defined accordingly:

$$u_{\tau i} = \sqrt{\frac{\tau_i}{\rho}}, \quad u_{\tau o} = \sqrt{\frac{\tau_o}{\rho}}, \quad u_{\tau g} = \sqrt{\frac{1}{\rho}\frac{\partial\bar{p}}{\partial x}}. \tag{6}$$

Throughout this paper, the subscript "$_i$" denotes the convex wall, "$_o$" the concave wall and "$_g$" the global variable.

To ascertain the accuracy and reliability of the present simulation, the mean velocity profile and turbulent intensities are compared with those of Moser & Moin (1987) and they show a good agreement.

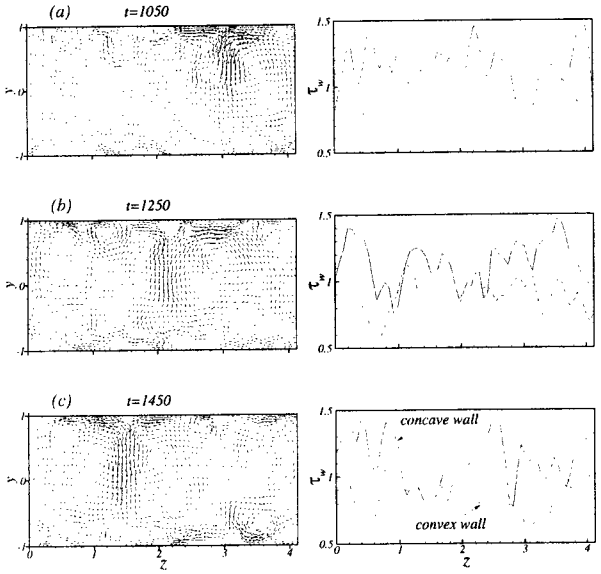

Figure 2: Streamwise averaged (v, w) vectors on (y, z)-plane and variation of the wall shear stress in the spanwise direction at (a) t=1050; (b) t=1250; (c) t=1450.

IDENTIFICATION OF TAYLOR-GÖTLER VORTICES

In general, Taylor-Götler vortices (TGVs) can be made stationary by introducing artificial disturbances upstream of the curved section (Moser & Moin, 1987). In the present computation, Taylor-Götler vortices themselves act as the analogous upstream disturbances by using the periodic boundary conditions in streamwise direction. Nothing can precludes them from moving in the spanwise direction. Accordingly, the strength and effects of the Taylor-Götler vortices are underestimated by conventional temporal average. In the present study, the drifting Taylor-Götler vortices in the spanwise direction are identified by adopting a conditional average.

Before describing the identification method used in present study, we first explain the "location of the drifting TGVs". As mentioned earlier, TGVs are large streamwise counter-rotating cells. Between the vortices, the flow away from the concave wall is relatively stronger than the flow towards the concave wall. At the boundaries between the vortices where the fluids move away from the concave wall, the boundary layer thickness is greatest and the skin friction is lowest (Moser & Moin, 1987). The streamwise averaged (v, w) vectors along with the spanwise variation of the

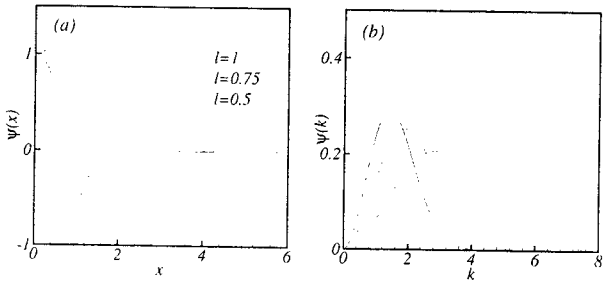

Figure 3: Marr wavelets and their Fourier coefficients.

streamwise averaged wall shear stress at three different time instants are displayed in Fig. 2. At $t = 1050$, the drifting TGVs is located at about $z = 3.0$, while it moves to $z = 2.2$ at $t = 1250$ and to $z = 1.4$ at $t = 1450$. Compared with the corresponding vector plots, the spanwise variations of the concave wall shear stress take local minimum values at the locations of TGVs. However, the local minimum points of $\partial u/\partial y|_{y=1}$ are not always equivalent to the locations of TGVs. This is because the wall information is firectly influenced by the near-wall small scale structures. According to the linear stability, a relationship between the maximum amplification wavelength (λ) and the curvature parameter (ϵ) is $\lambda^3 \sim \epsilon^4$. Usually the wavelength of the TGVs is of the order of channel width, which is much larger than the turbulent coherent structures. A multi-scale decomposition by the wavelet analysis can help us to distinguish the points of the TGVs from the streamwise vortices.

In present study, a continuous wavelet transform with Marr wavelets is employed to decompose the flow signals at chosen scale (Farge, 1992). The mother function of Marr wavelets is

$$\psi(z) = (1 - z^2)e^{-z^2/2}. \tag{7}$$

Its Fourier transform is

$$\hat{\psi}(k) = \frac{k^2}{\sqrt{2\pi}} e^{-k^2/2}. \tag{8}$$

The wavelets can be constructed from mother function by dilation and translation as

$$\psi_{lz'}(z) = l^{-\frac{1}{2}} \psi(\frac{z - z'}{l}), \tag{9}$$

where l and z' are the scale and position parameters, representing the dilation and translation of the wavelets respectively. Accordingly, their Fourier transform are

$$\hat{\psi}_{lz'}(k) = l^{\frac{1}{2}} \hat{\psi}(lk) e^{-ikz'}. \tag{10}$$

Fig. 3 shows Marr wavelets and their Fourier transforms at $l = 1, 0.75, 0.5$. We can see that the width of the wavelets decrease with decreasing the scale and the wave number band becomes wider and moves to the higher wave number side. The continuous wavelet transform of a function $f(z)$ is

$$\tilde{f}(l, z') = \int_{-\infty}^{+\infty} f(z)\psi^*_{lz'}(z)dz = \int_{-\infty}^{+\infty} \hat{f}(k)\hat{\psi}^*_{lz'}(k)dk. \tag{11}$$

The wavelength of the TGCVs can be estimated and the scale of the wavelet can then be determined. In the present study, the maximum amplification wavelength (λ) is estimated from the maximum energy spectra of the wavelet coefficients. In present study, $\epsilon = 0.0127$, the wavelength of TGVs is about $\lambda \simeq 4$, which satisfy the instability theory

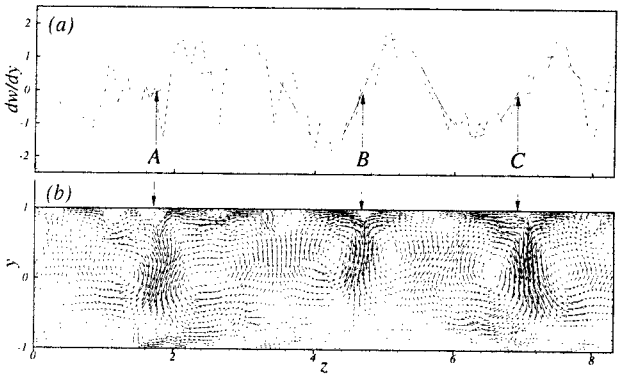

Figure 4: Using wavelet coefficients of $\partial w/\partial y|_w$ to identify Taylor-Götler vortices. (a) $\partial w/\partial y|_w$ and its wavelet coefficients; (b) (v, w) vectors.

(Saric, 1994). Accordingly, we can chose $l = 0.75$ in the wavelet analysis.

Also because the vortices are counter-rotating, at the outflow boundaries between TGVs, the spanwise velocity w equals to zero. Hence we can use the zero-crossing of $\partial w/\partial y|_{y=1}$ as well as the local minimum of $\partial u/\partial y|_{y=1}$ in the spanwise variation to identify the location of TGVs. Because the distribution of the local minimum of can be greatly influenced by wall actuation, for consistency, we use the zero-crossing of $\partial w/\partial y|_{y=1}$ to identify TGVs in controlled and uncontrolled flows.

Because the vortices are counter-rotating between the TGVs, the spanwise velocity (w) goes to zero near the wall. Hence, we can use the zero-crossing of $\partial w/\partial y|_{y=1}$ as well as the local minimum of $\partial u/\partial y|_{y=1}$ in the spanwise variation to identify the location of TGVs. Since the local minimum of $\partial u/\partial y|_{y=1}$ can be greatly influenced by wall actuation (Choi, Moin & Kim, 1994), the zero-crossing of $\partial w/\partial y|_{y=1}$ is employed in the present study. Fig. 4 shows an example of the identification by using the wavelet coefficients of $\partial w/\partial y|_{y=1}$. The dashed line in fig. 4(a) shows the distribution of streamwise averaged $\partial w/\partial y|_{y=1}$ in the spanwise direction and the solid line is its wavelet coefficients.

The dashed line is very fluctuating and has many zero-crossing points. The wavelet coefficient represents a filtered signal at the chosen scale. The corresponding (v, w) vectors in (y, z) plane are displayed in Fig. 4(b). Three zero-crossing points with a positive spanwise slope are detected, which are indicated by "A", "B" and "C", respectively. A closer inspection of the vector plots discloses that the locations of the TGVs are identified by the three points. Other three zero-crossing points with negative spanwise slope indicate the position between two TGVs at which the flow is directed toward the concave wall.

The method of identifying the TGVs is summarized as:

1. Calculate the spanwise distribution of the streamwise averaged $\partial w/\partial y|_{y=1}$;

2. Apply the wavelet transform for the above signal at the chosen scale;

3. Choose the zero-crossing points with positive spanwise slope of the wavelet coefficient.

The locations of TGVs at different time instants are shown in Fig. 5. There are two pairs of TGVs and the mean wavelength of the TGVs is $\lambda \simeq 4.0$. To get the statistical

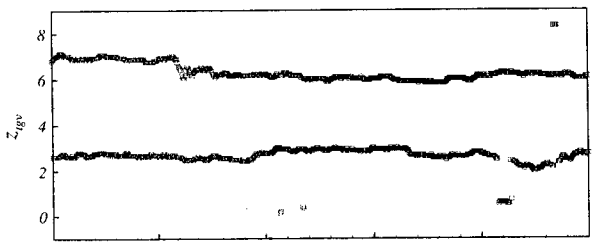

Figure 5: Trajectory of Taylor-Götler vortices.

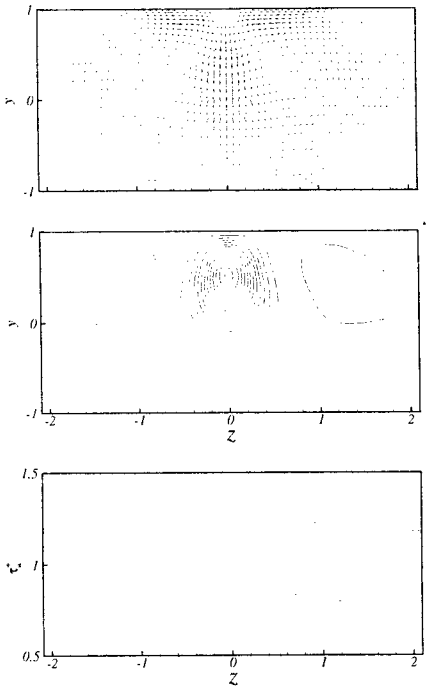

Figure 6: (v, w) vectors, Reynolds stress contours and variations of wall shear stress in the spanwise direction.

properties of TGVs, an ensemble average is performed. The ensemble average is taken along the center positions of the TGVs. The statistics are obtained by averaging the sample flow fields in the streamwise direction and in time. More than 1000 realizations of velocity and pressure in the whole computational domain are stored and averaged.

The ensemble averaged (v, w) vectors and Reynolds stress in (y, z) plane and the spanwise variations of the wall shear stress are displayed in Fig.6. It is seen that the concave wall shear stress reaches a minimum between TGVs, while the convex wall shear stress has a maximum at the corresponding position. In present study, the Reynolds number based on the bulk mean velocity is fixed at 2600, and the corresponding Reynolds number based on wall friction velocity is $Re_{\tau i} = 153$, $Re_{\tau o} = 182$ and $Re_{\tau} = 170$, respectively.

CONTROL OF TAYLOR-GÖTLER VORTICES

The role of near-wall streamwise vortices has been found to be very important in a wall-bounded turbulent flow. The downward sweep motion indeuced by streamwise vortices very near the wall is closely correlated with skin friction (Kim, 1987). Choi, Moin & Kim (1994) investigated an active control strategies for the purpose of drag reduction in

Case	Acting wall	Dr_g	Dr_l
2D v	convex	12.4	31.3
2D w	convex	12.2	28.6
2D v	concave	13.1	21.0
2D w	concave	14.5	23.2
1D v	concave	-19.6	-26.9
1D w	concave	-1.3	-0.9
1D w + 2D v	concave	11.9	20.4
1D w + 2D w	concave	7.9	14.4

Table 1: Drag reduction rate(%).

turbulent channel flow. The control algorithm is based on the input velocity at the wall, which is proportional and opposite to the instantaneous velocity at a location near the wall. By controlling either the normal or the spanwise velocity at the wall, they achieved $20 - 30\%$ reduction in the skin friction. In this section, a similar control algorithm is employed to attenuate the TGVs and to reduce the drag. In the following, we use "2Dv" and "2Dw" to denote two-dimensional controls by the wall blowing/suction velocity (v) and wall sliding velocity (w) at $y^+ \approx 10$, respectively. "1Dv" denotes one-dimensional control in the normal velocity (v) at $y^+ \approx 110$. It is seen that the normal velocity of the TGVs is maximum at $y^+ \simeq 110$. "1Dw" represents one-dimensional control in the spanwise velocity (w) at $y^+ \approx 26$, where the spanwise velocity of the TGVs is maximum. These one-dimensional controls aim at the attenuation of the TGVs.

The drag reduction rates under eight different controls are listed in Table 1. The drag reduction rate at each wall is measured by $Dr_l = (1 - \tau_c/\tau_{no}) \times 100$, where τ_{no} and τ_c are the mean shear stress at the wall before and after control. Since the drag reduction rates at the two walls are diffrent, a global drag reduction rate is defined by the mean streamwise pressure gradient, $Dr_g = [1 - (d\bar{p}/dx)_c/(d\bar{p}/dx)_{no}] \times 100$. Here $(d\bar{p}/dx)_{no}$ and $(d\bar{p}/dx)_c$ are the mean streamwise pressure gradient before and after control. By this definition, the constant mass flow rate is maintained. As shown in Table 1, the local drag reduction rates by "2D v" and "2D w" at the convex wall are larger than those at the concave wall. However, the global drag reduction rates at the convex wall are smaller than those at the concave wall. This is because the magnitude of friction drag at the concave wall is larger than that at the convex wall. It is seen that "2D w" at the concave wall is slightly more effective than "2D v" at the concave wall. As mentioned earlier, the main goal of the control is to attenuate the TGVs by one-dimensional active cancellation. As shown in Table 1, the cancellation by "1D v" and "1Dw" are effective in suppressing the TGVs. However, the local and global friction drags at the wall are not reduced, even increased. In particular, "1Dv" gives a significant increase of drag, while "1D w" is weak. Although the TGVs are suppressed by "1Dv", the friction drag near the wall is then increased by the high momentum actuation by "1Dv" (Hammond, 1998). To achieve the suppression of the TGVs as well as the drag reduction at the wall, a combined control is proposed in present study. As shown in Table 1, an optimum choice is "1D w + 2D v" at the concave wall. This gives a global drag reduction by 11.9% and a local drag reduction by 20.4%, respectively.

To see the influences of the eight different controls on TGVs, (u, w) vectors, Reynolds stresses and wall shear stresses are displayed in Fig. 7-10. These are obtained by the afore-stated ensemble averaging in the streamwise direction and in time. For "2Dv" at the concave wall in Fig. 7 (a), the

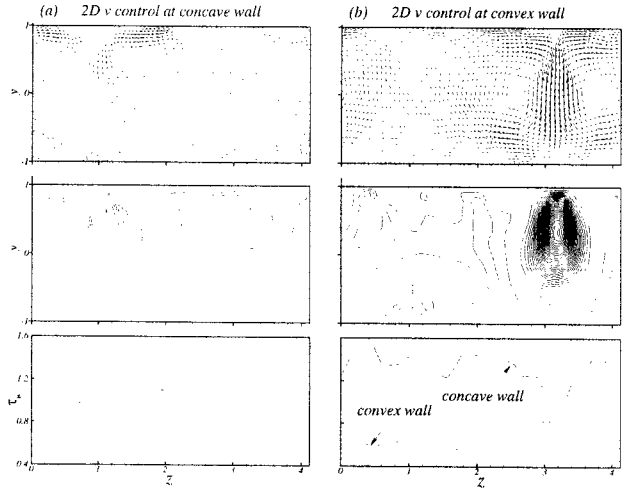

Figure 7: (v, w) vectors and uv contours in (y, z)-plane, and variations of wall shear stress in spanwise direction for flows under "2Dv" at (a) concave wall and (b) convex wall.

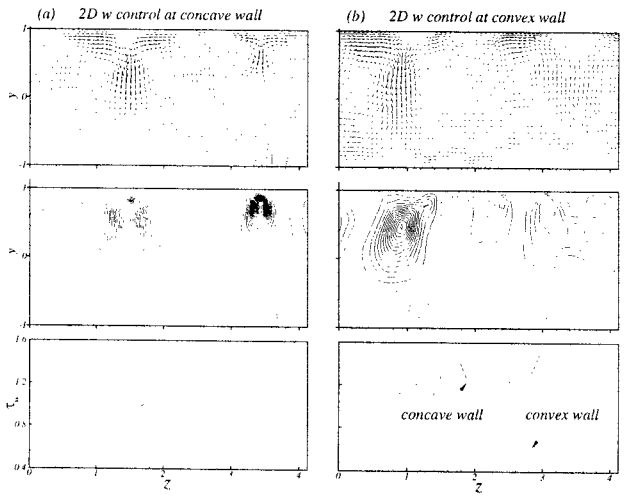

Figure 8: (v, w) vectors and uv contours in (y, z)-plane, and variations of wall shear stress in spanwise direction for flows under "2Dw" at (a) concave wall and (b) convex wall.

TGVs are weakened and the corresponding Reynolds stress is also attenuated. The shear stress at the concave wall is reduced similar to the level at the convex wall. There is no sharp local minimum in the spanwise variation of wall shear stress between the TGVs. Figure 7 (b) shows the results of "2Dv" at the convex wall. The TGVs are strengthened and shifted closer to the convex wall. The Reynolds stress is also intensified. Not only the local minimum in the spanwise variation of concave wall shear stress, but also the local maximum in the spanwise variation of the convex wall shear stress are found, indicating that the blowing and suction at the convex wall act as an increase of the curvature in the previous section. Fig. 8 shows the results of "2Dw". The sliding velocity (w) either at the concave wall or at the convex wall can not effectively give an influence on the strength and the position of the TGVs. The results of "1Dv" and "1Dw" at the concave wall are shown in Fig. 9. The TGVs disappear completely under "1D v", as shown in Fig. 9(a). This is because an active cancellation is effectively performed at $y^+ = 110$ by the actuating velocities.

For "1D w", the TGVs are also greatly suppressed in

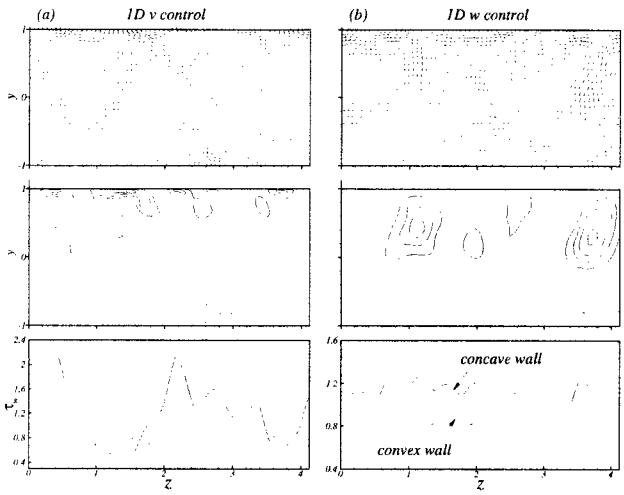

Figure 9: (v, w) vectors and uv contours in (y, z)-plane, and variations of wall shear stress in spanwise direction for flows under (a) "1Dv" and (b) "1Dw" at concave wall.

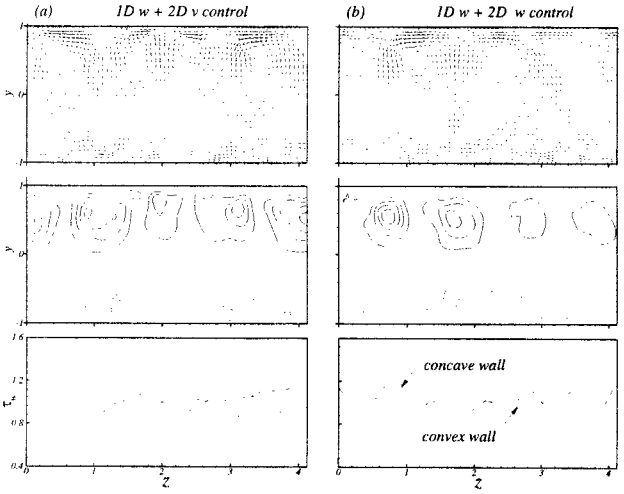

Figure 10: (v, w) vectors and uv contours in (y, z)-plane, and variations of wall shear stress in spanwise direction for flows under (a) "1Dw+2Dv" and (b) "1Dw+2Dw" at concave wall.

Fig. 9 (b). As mentioned earlier, "1Dw" is effective in suppressing the TGVs and "2Dv" and "2Dw" are effective in reducing the wall friction. The combined controls on the TGVs are displayed in Fig. 10. It is seen that "1Dw + 2Dv" at the concave wall is similar to " 1Dw + 2Dw" at the concave wall. They both make the TGVs break up to smaller vortices, and weaken their strengthes and contributions to Reynolds stress.

In the present curved channel flow, the mean wall friction can be decomposed into three parts: 'laminar', 'TGV' and 'turbulence', respectively (Moser & Moin, 1987). The laminar part is the viscous shear stress of laminar flow at the same mass flux, and it is irreducible by the flow manipulation. In turbulent flow, the Reynolds stress $\overline{u'v'}$ can be decomposed into

$$\overline{u'v'} = \overline{(\tilde{u} - \bar{u})(\tilde{v} - \bar{v})} + \overline{u''v''} \qquad (12)$$

where $\overline{(\tilde{u} - \bar{u})(\tilde{v} - \bar{v})}$ represents the contribution of the TGVs and $\overline{u''v''}$ denotes the contribution of turbulence. The mean friction is obtained by solving the mean momentum equation (Moser & Moin, 1987).

	Case	Lmn	Tur	TGV	Tot
Concave	no control	1.14	3.03	0.70	4.87
	2D v	1.14	2.33	0.43	3.91
	1Dw + 2Dv	1.14	2.50	0.20	3.84
Convex	no control	1.16	2.25	0.13	3.54
	2D v	1.16	2.16	0.11	3.44
	1Dw + 2Dv	1.16	2.34	0.05	3.56

Table 2: Contributions to drag ($\times 10^{-3}\rho U_m^2$).

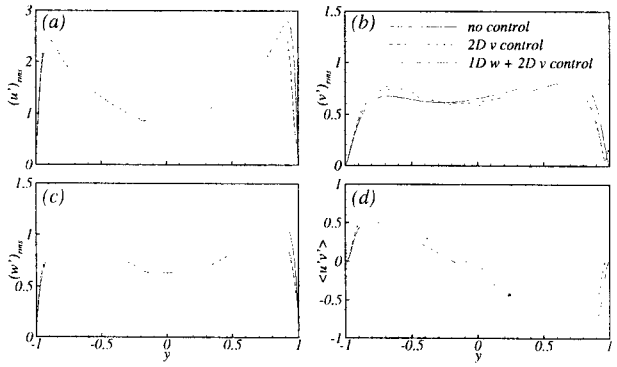

Figure 11: Influence of "2Dv" and "1Dw+2Dv" to root-mean-square of velocity fluctuations and Reynolds stress. (a) u'_{rms}; (b) v'_{rms}; (c) w'_{rms} and (d) $\overline{u'v'}$.

When the active cancellations are applied at the concave wall, the contributions of the three parts to the mean wall friction are summarized in Table 2. At the concave wall, both 'turbulence' and 'TGV' are suppressed by "2Dv" and "1Dw+2Dv", compared with 'no control'. In particular, 'TGV' is greatly suppressed by "1Dw+2Dv". The portion of 'TGV' to the total wall friction is very small when "1Dw+2Dv" is applied. However, the role of 'TGV' at the convex wall is relatively smaller than that at the concave wall. It is seen that "1Dw+2Dv" is not effective in reducing the mean wall friction at the convex wall.

The statistical contributions of the TGVs to the velocity components and Reynolds stress under "2D v" and "1Dw+2Dv" at the concave wall are displayed in Fig.11. For comparison, the results of 'no control' are also included. It is generally seen that "1Dw+2Dv" is more effective in suppressing the turbulent intensities and Reynolds stress. The suppression by "2Dv" is also apparent. The root mean square of total turbulent velocity fluctuations and Reynolds stress are shown in Fig.11 to further depict the influence of "2Dv" and "1Dw+2Dv". By the active cancellations, turbulent fluctuations are suppressed near the concave wall, while they are enhanced at the concave wall. The profiles are less asymmetric with respect to the channel center. The asymmetric profiles indicate that the streamwise and normal fluctuations are mutually correlated on the concave side rather than on the convex side. This is attribute to the contributions of the TGVs (Moser & Moin, 1987). Due to the present cancellations, the asymmetry is recovered to the symmetry. For example, the zero-crossing point in the Reynolds stress of 'no control' is observed at $y = -0.2$ in Fig.11(d), while it moves to $y = -0.1$ in the cancellation.

CONCLUSIONS

A new algorithm has been proposed for identifying the drifting Taylor-Götler vortices in turbulent curved channel flow. A continuous wavelet transform with Marr wavelets was employed to decompose the flow signals at a chosen length scale. The positions of the Taylor-Götler vortices were the zero-crossing points with a positive spanwise slope of the wavelet coefficients. To suppress the Taylor-Götler vortices near the concave wall, one-dimensional active cancellation was applied. The one-dimensional active cacellation in the wall normal direction was effective to attenuate the Taylor-Götler vortices. However, due to the high momentum actuation at the wall, the friction drag near the wall was increased. To achieve the suppression of the Taylor-Götler vortices as well as the wall friction reduction, a combined control was imposed at the concave wall. The drag reduction was estimated by 11.9% globally.

ACKNOWLEDGEMENT

This research was supported by a grant from the National Research Laboratory of the Ministry of Science and Technology, Republic of Korea. The first author acknowledges the support of the Korea Science and Engineering Foundation and the Natural Science Foundation of China (Grants 10072032 and 10232020).

REFERENCES

Bradshaw, P., 1973, "Effects of streamline curvature on turbulent flow", AGAR-Dograph No. 169, AGARD, 7 Rue Acelle, 92200, Neuilly Sur Seine, France.

Choi H., Moin P., and Kim J., 1994, "Active turbulence control for drag reduction in wall-bounded flows", *J. Fluid Mech.*, Vol. 262, pp. 75-1101.

Farge M., 1992, "Wavelet transforms and their applications to turbulence", *Annu. Rev. Fluid Mech.* vol. 24, pp. 395-457.

Götler H., 1940, "On the three-dimensional instability of laminar boundary layers on concave walls", NACA TM 1375.

Hammond, E.P., Bewley, T.R., and Moin, P., 1998, "Observed mechanisms for turbulence attenuation and enhancement in opposition-controlled wall-bounded flows", *Phys. Fluids*, vol. 10, pp. 2421-2423.

Karniadakis G.E., Israeli M., and Orszag S.A., 1991, "High-order splitting methods for the incompressible Navier-Stokes equations", *J. Comput. Phys.*, vol. 97, pp. 414-443.

Kim, J., Moin, P., and Moser, R.K., 1987, "Turbulence statistics in fully developed channel flow at low Reynolds number", *J. Fluid Mech.*, vol. 177, pp. 133-166.

Lund, T.S., and Moin, P., 1996, "Large-eddy simulation of a concave wall boundary layer", *Int. J. Heat Fluid Flow*, vol. 17, pp. 290-295.

Moser R.D., and Moin P., 1987, "The effects of curvature in wall-bounded turbulent flows", *J. Fluid Mech.*, vol. 175, pp. 479-510.

Patel V.C., and Sotiropoulos F., 1997, "Longitudinal curvature effects in turbulent boundary layers", *Prog. Aerospace Sci.*, vol. 33, pp. 1-70.

Saric, W.S., 1994, "Götler vortices", *Annu. Rev. Fluid Mech.*, vol. 26, pp. 379-409.